Weak and strong coupling in a two-lane asymmetric exclusion process

Rui Jiang,[1] Mao-Bin Hu,[1,2] Yong-Hong Wu,[2] and Qing-Song Wu[1]
[1]*School of Engineering Science, University of Science and Technology of China, Hefei 230026, China*
[2]*Department of Mathematics and Statistics, Curtin University of Technology, Perth WA6845, Australia*
(Received 1 November 2007; revised manuscript received 6 April 2008; published 29 April 2008)

This paper studies a two-lane totally asymmetric simple exclusion process, in which particles could jump between the two lanes with asymmetric rates. In the weak coupling situation, the rates are inversely proportional to system size L. The appearance of localized shock in one lane and the discontinuous phase transition as revealed by Juhász [Phys. Rev. E **76**, 021117 (2007)] are also reproduced. The density profiles and phase diagrams are constructed in the hydrodynamic limit, by numerically solving the steady state equations. The phase diagram in our model exhibits asymmetry, which is different from the symmetric one in Juhász's model. We have studied the phase boundary and discontinuous line analytically. The analytical results are in good agreement with that obtained from numerical integration. We also study the strong coupling situation, in which the lane changing rates are independent of L. Results completely different from that arising from weak coupling are presented. Furthermore, features different from that of the model presented by Pronina and Kolomeisky [Physica A **372**, 12 (2006)] are revealed.

DOI: 10.1103/PhysRevE.77.041128 PACS number(s): 02.50.Ey, 47.11.Qr, 05.60.−k

I. INTRODUCTION

In recent years, the asymmetric simple exclusion process (ASEP), which is a discrete model that describes the stochastic dynamics of multiparticle transport along one-dimensional lattices, has attracted the interest of physicists, because it plays an important role in understanding various nonequilibrium phenomena in chemistry, physics, and biology [1–11].

In an ASEP, each lattice site can be either empty or occupied by a single particle. Particles interact only through hard core exclusion potential. If particles can only move in one direction, we have the totally asymmetric simple exclusion process (TASEP). In contrast, in a partially asymmetric exclusion process, particles are allowed to hop into both directions, but with different rates.

Recently, the coupling of ASEP with other processes has led to many unusual and unexpected phenomena. For example, Parmeggiani *et al.* investigated the interplay of TASEP with the creation and annihilation of particles in the bulk. The phenomenon of localized density shock was produced and was explained by applying a phenomenological domain wall theory [12–15]. On the other hand, to analyze more realistic phenomena, the multilane ASEP has been developed to model the transport along parallel channels [16–25]. For example, Popkov *et al.* studied the two-lane ASEP in which the hopping rates of particles on one lane depend on the configuration on the other lane [16]. The two-lane TASEP where particles are allowed to jump between two lanes are also widely studied. Both symmetric jumping and asymmetric jumping are considered. The two-way traffic on the two lane TASEP has also been investigated [23–25].

In a recent paper, Pronina and Kolomeisky studied asymmetric coupling in a two-lane TASEP [20]. They found seven phases in the case of full asymmetric coupling. Nevertheless, their work only studies strong coupling, in which the lane changing rates are independent of system size L. Many works show that weak coupling, in which the rates are inversely proportional to L, could lead to various unusual and unexpected phenomena [12–15,25]. Therefore in this paper, we investigate both weak and strong coupling in a two-lane asymmetric TASEP.

The paper is organized as follows. In Sec. II we give a brief description of the model. In Sec. III, the results of weak coupling are discussed in detail. In Sec. IV, we present the results of strong coupling. We give our conclusions in Sec. V.

II. MODEL

Our model is defined in a two-lane lattice of $L\times 2$ sites, where L is the length of a lane. We introduce an occupation variable $\tau_{\ell,i}$ where $\tau_{\ell,i}=1$ (or $\tau_{\ell,i}=0$) indicates that the state of the ith site in lane ℓ (A or B) is occupied (or vacant). We apply the following dynamical rules (also see Fig. 1). For each time step, a site (ℓ,i) is chosen at random.

1. Subcase $i=1$: (i) If $\tau_{\ell,1}=0$, a particle enters the system with rate α. (ii) If $\tau_{\ell,1}=1$ and $\tau_{\ell,2}=0$, then the particle in the site of $(\ell,1)$ moves into site $(\ell,2)$ with unit rate. (iii) If $\tau_{\ell,1}=1$ and $\tau_{\ell,2}=1$, then the particle in the site of $(\ell,1)$ stays there. No lane change occurs here.

2. Subcase $i=N$. If $\tau_{\ell,N}=1$, the particle leaves the system with rate β. No lane change occurs.

3. Subcase $1<i<N$. If $\tau_{\ell,i}=1$, the particle moves into site $(\ell,i+1)$ with unit rate if $\tau_{\ell,i+1}=0$. Otherwise, it changes to the other lane with rate ω_ℓ if the corresponding site on the other lane is empty.

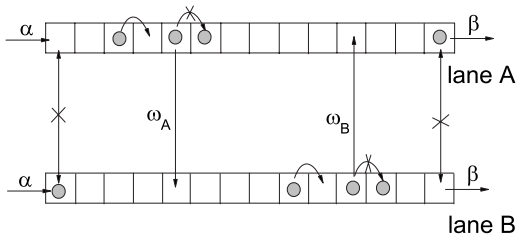

FIG. 1. Sketch of the two lane TASEP. The arrow shows allowed hopping and the cross shows prohibited hopping.

Note that our model is different from the model of Pronina and Kolomeisky [20], in which the particles change lane first if the corresponding site on the other lane is empty. This difference leads to qualitatively different results (see Sec. IV). We argue that our model is relevant with such transport phenomena as vehicular flow and motor proteins because normally a vehicle or a molecular motor does not change lanes if unhindered by a preceding one.

III. WEAK COUPLING

In this section, we study the situation arising from weak coupling, in which the lane changing rates ω_A and ω_B are inversely proportional to L. We denote $\omega_A L=\Omega_A$, $\omega_B L=\Omega_B$, and $K=\Omega_B/\Omega_A$. Here Ω_A and Ω_B are constants.

A. Phase diagram and density profile

Figure 2 shows phase diagrams under different values of Ω_A with $\Omega_B=0$. When Ω_A is small, the phase diagram is classified into five regions. In region HH, both lanes are in high density; In region LL, both lanes are in low density; In region HL, lane B is in high density and lane A is in low density. In regions HS and SL, a shock appears in the system. In region HS, lane B is in high density and a shock appears in lane A; In region SL, a shock appears in lane B and lane A is in low density. Regions HS and SL are well separated by region HL. Figure 3 shows the typical density profiles in the five regions.

With the increase of Ω_A, regions LL and HH shrink, region HL expands, region HS shifts downwards, and region SL shifts toward the left. With the further increase of Ω_A, regions HS and SL also shrink. Note that region HS shrinks much faster than region SL. When Ω_A is sufficiently large, regions HS and SL disappear. Our simulations show that these two regions do not disappear simultaneously. After regions HS and SL disappear, boundary 1 between HL and HH as well as boundary 2 between HL and LL does not change with Ω_A. Moreover, boundaries 1 and 2 are symmetric with respect to the line $\alpha=\beta$.

Figure 4 shows phase diagrams under different values of Ω_A with $\Omega_B/\Omega_A=0.01$. The results are different from that of $\Omega_B=0$. (i) First, regions HS and SL are not separated by region HL. (ii) Regions HS and SL do not disappear even if Ω_A is very large. (iii) The phase diagram is not symmetric with respect to the line $\alpha=\beta$ when Ω_A is very large. (iv) The boundary between regions HS and HL becomes a straight line when Ω_A is sufficiently large.

Furthermore, a straight discontinuous line appears in region HS when Ω_A is larger than a critical value Ω_A^{c1} [dashed line in Fig. 4(b)]. When crossing the discontinuous line, a jump of the location of the shock occurs [Figs. 5(d)–5(f)]. On the discontinuous line, there is no shock in the system, and the density profiles are characterized by a segment of constant densities [Fig. 5(d)].

When Ω_A is larger than a second critical value Ω_A^{c2}, a second discontinuous line appears in region SL [Fig. 4(c)]. The density profiles when crossing the discontinuous line are shown in Figs. 5(a)–5(c). The two discontinuous lines expand with the increase of Ω_A. When Ω_A is extremely large, the discontinuous line intersects with $\alpha=\beta$ in region HS and it intersects with the boundary between regions SL and HL in region SL.

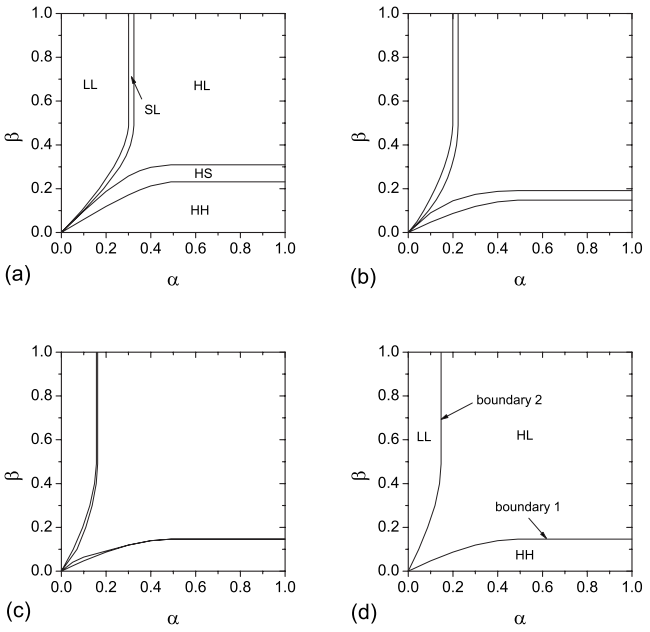

FIG. 2. Phase diagrams under different values of Ω_A with $\Omega_B=0$. (a) $\Omega_A=1$; (b) $\Omega_A=10$; (c) $\Omega_A=100$; (d) $\Omega_A=10\,000$. The boundaries are obtained by numerical integration of Eqs. (8) and (9) with proper boundary conditions.

We check the location of shock when crossing the line $\alpha=\beta$, which is shown in Fig. 6. One can see when β is slightly smaller than α, the shock is on lane A [Fig. 6(a)]. The shock position tends to $x_{\min,1}$ when $\beta\to\alpha$. When β is slightly larger than α, the shock is on lane B [Fig. 6(b)]. The shock position tends to $x_{\min,2}$ when $\beta\to\alpha$. Note that different from the two-way traffic situation in Ref. [25], $x_{\min,1}\neq x_{\min,2}$ in this case. Exactly on the line $\alpha=\beta$, the shocks in both lanes are delocalized and perform a stochastic motion in the domain $[x_{\min,1},1]$ on lane A and in the domain $[0,x_{\min,2}]$ on lane B.

Figure 7 shows phase diagrams under different values of Ω_A with $\Omega_B/\Omega_A=0.1$. Similar results as in the case of $\Omega_B/\Omega_A=0.01$ are identified. Note that the boundary between regions SL and HL also gradually becomes straight when Ω_A is large. As a result, the discontinuous line also intersects with $\alpha=\beta$ in region SL.

We have compared our results from that in Ref. [25] (see also Ref. [26]). They are similar in the following aspects: (i) Five regions are classified in the phase diagram, which exhibits similar five phases; (ii) the discontinuous phase transition is observed in SL and HS. However, there are differences between the results: (i) the discontinuous line is a straight line in our system, while it is not straight in Ref. [25] (this is explained in Sec. III C 5); (ii) more importantly, the phase diagram and the discontinuous line in Ref. [25] are symmetric. In contrast, they are asymmetric in our system. In Sec. III C, we will study the phase boundaries analytically.

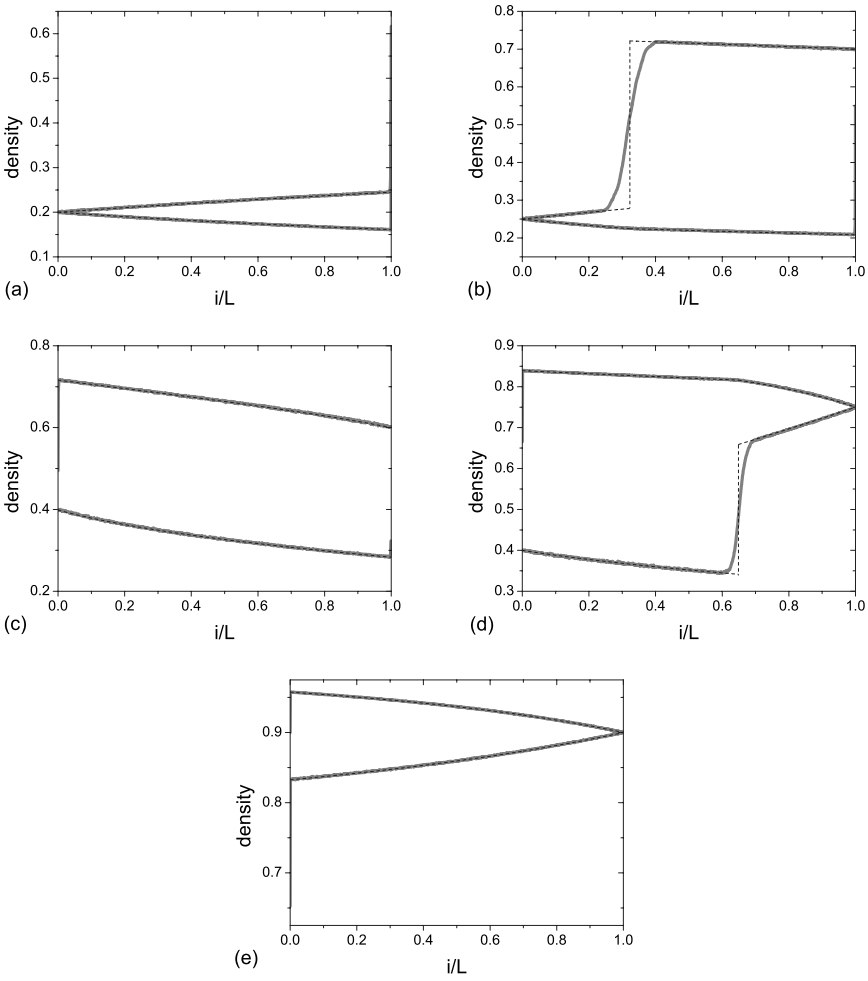

FIG. 3. Typical density profiles in region (a) LL; (b) SL; (c) HL; (d) HS; (e) HH. The parameters are $\Omega_A=1$, $\Omega_B=0, L=10\,000$. In (a) $\alpha=0.2$, $\beta=0.3$; (b) $\alpha=0.25$, $\beta=0.3$; (c) $\alpha=0.4$, $\beta=0.4$; (d) $\alpha=0.4$, $\beta=0.25$; (e) $\alpha=0.4$, $\beta=0.1$. The dashed thin lines are analytical results obtained by numerical integration and the solid thick lines are simulation results.

B. Hydrodynamic mean field analysis

In this subsection, a hydrodynamic mean field analysis of the density profiles is carried out. We restrict our discussion in the range $\alpha \leq 0.5$ and $\beta \leq 0.5$, because the effective boundary conditions are $\alpha_{eff}=\min(\alpha,1/2)$ and $\beta_{eff}=\min(\beta,1/2)$. This is because in the TASEP, maximum current phase is achieved when $\alpha>1/2$ and $\beta>1/2$, in which the current is limited by the maximal carrying capacity in the bulk.

It is well known that driven diffusive systems combined with a weak bulk nonconserving process are described by the partial differential equation [15],

$$\frac{\partial \rho(x,\tau)}{\partial \tau} + \frac{\partial J[\rho(x,\tau)]}{\partial x} = S, \tag{1}$$

where ρ is the local density, $J(\rho)=\rho(1-\rho)$ is the local current, $\tau=t/L$ is the rescaling time, S is the source term related to the nonconserving process. As a result, we have

$$\frac{\partial \rho_A}{\partial \tau} + \frac{\partial J_A}{\partial x} = -\Omega_A \rho_A^2 (1-\rho_B) + \Omega_B \rho_B^2 (1-\rho_A) \tag{2}$$

for lane A and

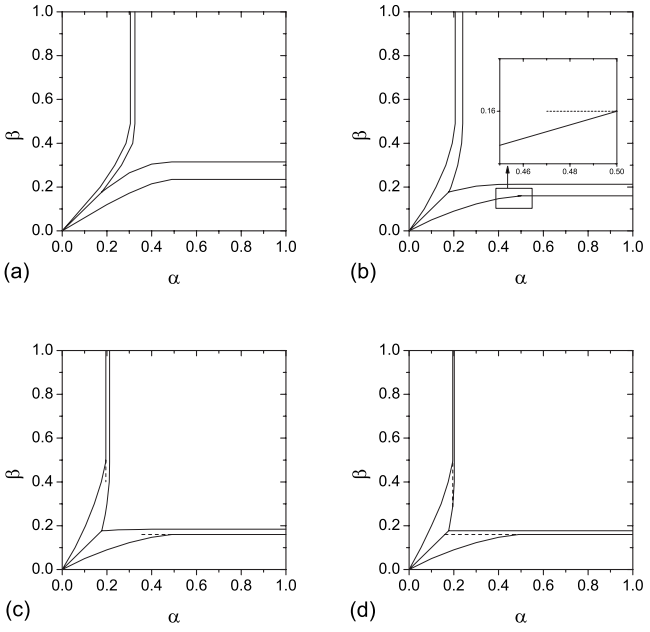

FIG. 4. Phase diagrams under different values of Ω_A with $\Omega_B/\Omega_A=0.01$. (a) $\Omega_A=1$; (b) $\Omega_A=10$; (c) $\Omega_A=40$; (d) $\Omega_A=10\,000$. The boundaries are obtained by numerical integration of Eqs. (8) and (9) with proper boundary conditions.

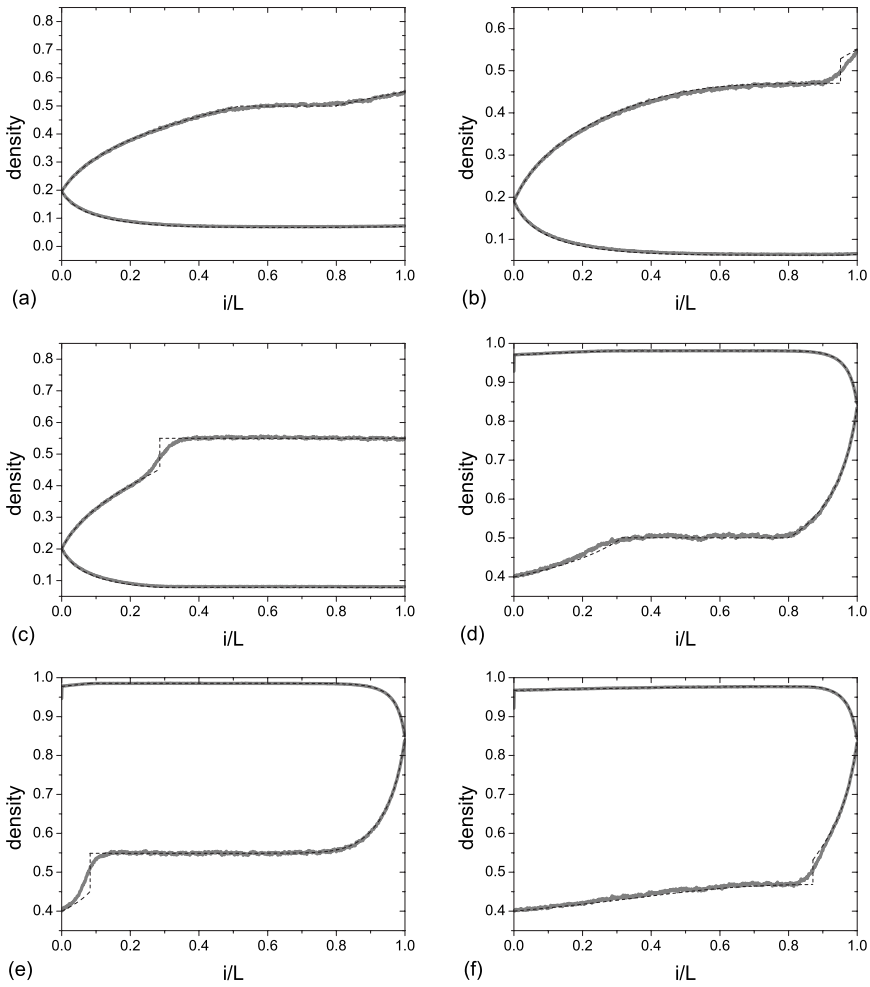

FIG. 5. Density profiles near the discontinuous line. The parameters are $\Omega_A=40$, $K=0.01$, $L=10\,000$. (a) $\alpha=0.1947$, $\beta=0.45$; (b) $\alpha=0.19$, $\beta=0.45$; (c) $\alpha=0.2$, $\beta=0.45$; (d) $\alpha=0.4$, $\beta=0.16$; (e) $\alpha=0.4$, $\beta=0.155$; (f) $\alpha=0.4$, $\beta=0.162$.

$$\frac{\partial \rho_B}{\partial \tau} + \frac{\partial J_B}{\partial x} = \Omega_A \rho_A^2 (1-\rho_B) - \Omega_B \rho_B^2 (1-\rho_A) \tag{3}$$

for lane B. In the steady state, we have $\partial \rho_A/\partial \tau = \partial \rho_B/\partial \tau = 0$. Therefore the density profiles $\rho_A(x)$ and $\rho_B(x)$ satisfy the coupled differential equations

$$(1-2\rho_A)\frac{\partial \rho_A}{\partial x} + \Omega_A \rho_A^2 (1-\rho_B) - \Omega_B \rho_B^2 (1-\rho_A) = 0, \tag{4}$$

$$(1-2\rho_B)\frac{\partial \rho_B}{\partial x} - \Omega_A \rho_A^2 (1-\rho_B) + \Omega_B \rho_B^2 (1-\rho_A) = 0. \tag{5}$$

Since the total current

$$J = \rho_A(1-\rho_A) + \rho_B(1-\rho_B) \tag{6}$$

is a constant, we have

$$\rho_B = \frac{1 \pm \sqrt{1-4[J-\rho_A(1-\rho_A)]}}{2}. \tag{7}$$

Substituting Eq. (7) into Eq. (4), we have

$$(1-2\rho_A)\frac{\partial \rho_A}{\partial x} + \Omega_A \rho_A^2 \left(1 - \frac{1 \pm \sqrt{1-4[J-\rho_A(1-\rho_A)]}}{2}\right) - \Omega_B \left(\frac{1 \pm \sqrt{1-4[J-\rho_A(1-\rho_A)]}}{2}\right)^2 (1-\rho_A) = 0. \tag{8}$$

Similarly, we have

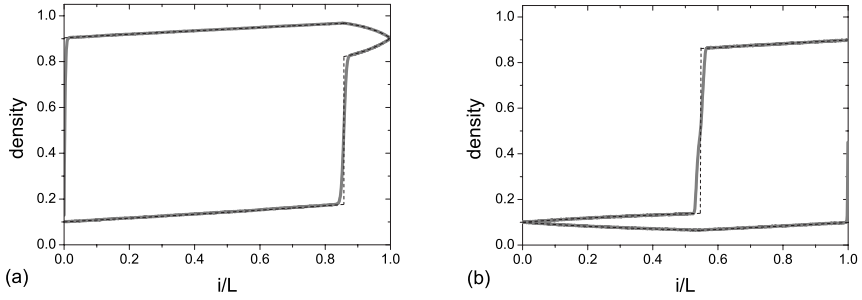

FIG. 6. Density profiles near the line $\alpha=\beta$. The parameters are $\Omega_A=10$, $K=0.01$, $L=10\,000$. (a) $\alpha=0.1$, $\beta=0.098$; (b) $\alpha=0.1$, $\beta=0.101$.

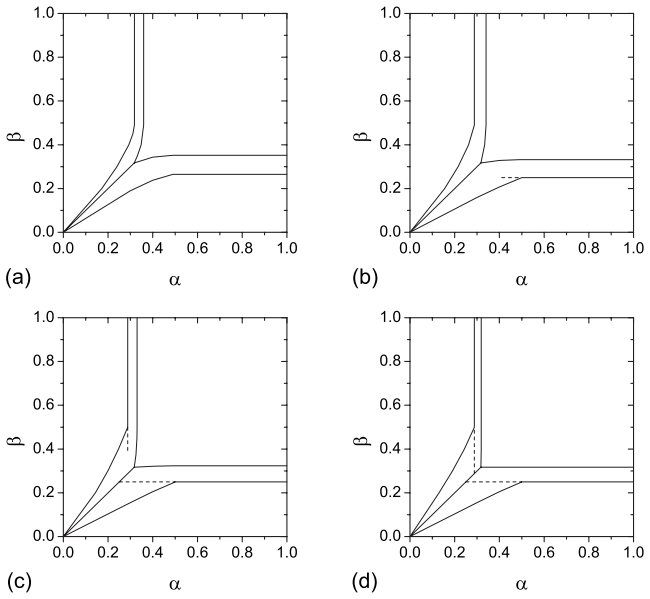

FIG. 7. Phase diagrams under different values of Ω_A with $\Omega_B/\Omega_A=0.1$. (a) $\Omega_A=1$; (b) $\Omega_A=2.5$; (c) $\Omega_A=5$; (d) $\Omega_A=100$. The boundaries are obtained by numerical integration of Eqs. (8) and (9) with proper boundary conditions.

$$(1-2\rho_B)\frac{\partial \rho_B}{\partial x}-\Omega_A\left(\frac{1\pm\sqrt{1-4[J-\rho_B(1-\rho_B)]}}{2}\right)^2(1-\rho_B)+\Omega_B\rho_B^2\left(1-\frac{1\pm\sqrt{1-4[J-\rho_B(1-\rho_B)]}}{2}\right)=0. \quad (9)$$

Equations (8) and (9) could be numerically integrated together with proper boundary conditions as follows:

$$\rho_A(0)=\min(\alpha,1/2), \quad (10)$$

$$\rho_B(0)=\min(\alpha,1/2), \quad (11)$$

$$\rho_A(1)=\max(1-\beta,1/2), \quad (12)$$

$$\rho_B(1)=\max(1-\beta,1/2). \quad (13)$$

1. In the LL phase, the total current $J=2\alpha(1-\alpha)$. The "−" is used in Eqs. (8) and (9) together with boundary conditions (10) and (11). In this case, the boundary layers exist on the right boundary on both lanes [Fig. 3(a)].

2. In the HH phase, the total current $J=2\beta(1-\beta)$. The "+" is used in Eqs. (8) and (9) together with boundary conditions (12) and (13). In this case, the boundary layers exist on the left boundary on both lanes [Fig. 3(e)].

3. In the SL phase, the total current $J=2\alpha(1-\alpha)$, and a shock appears on lane B. Denote the solutions on the two sides of the shock as $\rho_{B,l}(x)$ and $\rho_{B,r}(x)$; we obtain $\rho_{B,l}(x)$ by integrating Eq. (9) with "−" from the left boundary with boundary condition (11), and obtain $\rho_{B,r}(x)$ by integrating Eq. (9) with "−" from the right boundary with boundary condition (13). The position of the shock x_s, is implicitly given by $\rho_{B,l}(x_s)=1-\rho_{B,r}(x_s)$. The density profile on lane A is then calculated from the counterpart of Eq. (7) with "−", i.e., $\rho_A=\frac{1-\sqrt{1-4[J-\rho_B(1-\rho_B)]}}{2}$. In this case, a boundary layer exists on the right boundary on lane A [Fig. 3(b)].

4. In the HS phase, the total current $J=2\beta(1-\beta)$, and a shock appears on lane A. Denote the solutions on the two sides of the shock as $\rho_{A,l}(x)$ and $\rho_{A,r}(x)$; we obtain $\rho_{A,l}(x)$ by integrating Eq. (8) with "+" from the left boundary with boundary condition (10), and obtain $\rho_{A,r}(x)$ by integrating Eq. (8) with "+" from the right boundary with boundary condition (12). The position of the shock x_s is implicitly given by $\rho_{A,l}(x_s)=1-\rho_{A,r}(x_s)$. The density profile on lane B is then calculated from Eq. (7) with "+," i.e., $\rho_B=\frac{1+\sqrt{1-4[J-\rho_A(1-\rho_A)]}}{2}$. In this case, a boundary layer exists on the left boundary on lane B [Fig. 3(d)].

5. In the HL phase, the total current J needs to be obtained iteratively until self-consistency is attained [27]. We integrate Eq. (9) with "−" from the right boundary with boundary condition (13). If $\rho_{B,r}(0)$ obtained from the integration satisfies $\rho_{B,r}(0)[1-\rho_{B,r}(0)]+\alpha(1-\alpha)=J$, then we have the converged result. In this case, a boundary layer exists on the left boundary on lane B and the other boundary layer exists on the right boundary on lane A [Fig. 3(c)].

Figures 3, 5, and 6 show the density profiles from hydrodynamic mean field analysis. They are in good agreement with simulation results.

C. Phase boundaries and discontinuous lines

In this subsection, we investigate the phase boundaries and discontinuous lines analytically. The analytical expression can be found when Ω_A is sufficiently large. This is because, as shown below, $\frac{\partial \rho_B}{\partial x}|_{x=1}$ or $\frac{\partial \rho_A}{\partial x}|_{x=0}$ equal to zero (or are extremely close to zero) on corresponding boundaries. When Ω_A is small, $\frac{\partial \rho_B}{\partial x}|_{x=1}$ and $\frac{\partial \rho_A}{\partial x}|_{x=0}$ always remarkably deviate from zero on corresponding boundaries (or on part of

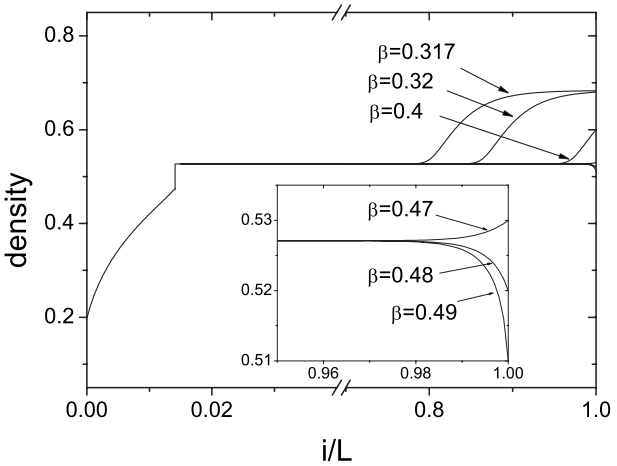

FIG. 8. Density profiles on lane B in the SL phase. The parameters are $\alpha=0.198$, $K=0.01$, $\Omega_A=1000$. The results are obtained from numerical integration of hydrodynamic mean field equations. β only affects density profiles near the right boundary. Here $\beta_{c1}\approx 0.317$, $\beta_{c2}\approx 0.472$. The inset shows details near the right boundary.

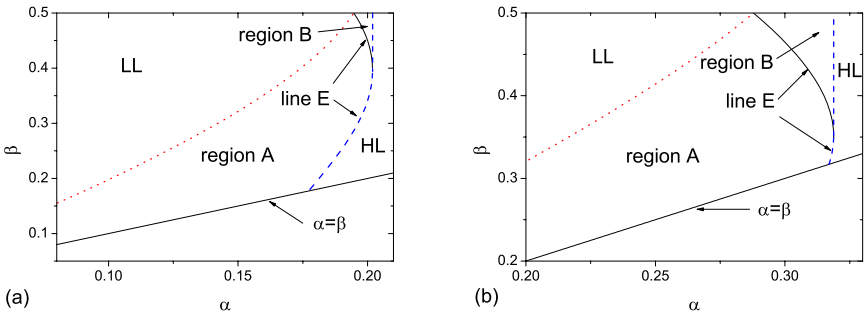

FIG. 9. (Color online) Boundary between SL and HL (blue dashed line). Boundary between LL and SL (red dotted line) is also shown, which is obtained from Eq. (15). (a) $K=0.01$; (b) $K=0.1$.

the boundaries). As a result, one cannot find an analytical expression at a small value of Ω_A.

We also need to point out that when Ω_A increases from a small value, the boundaries tend to the limiting ones (i.e., ones corresponding to sufficiently large Ω_A) with different speeds. For instance, at $K=0.005$, the boundary between HH and HS is almost identical to the limiting one when $\Omega_A=15$. However, the boundary between HS and HL still notably deviates from the limiting one even if $\Omega_A=150$.

1. Boundary between LL and SL

When Ω_A is sufficiently large, density profile on lane B is flat at the right boundary (i.e., $\frac{\partial \rho_B}{\partial x}|_{x=1}=0$) on the boundary between LL and SL. Substituting this into Eq. (9) (note that "–" needs to be used because lane A is in low density), we have

$$\Omega_A\left(\frac{1-\sqrt{1-4[J-\rho_B(1-\rho_B)]}}{2}\right)^2(1-\rho_B) = \Omega_B\rho_B^2\left(1-\frac{1-\sqrt{1-4[J-\rho_B(1-\rho_B)]}}{2}\right). \quad (14)$$

Furthermore, we have $\rho_B|_{x=1}=\beta$ on the boundary. Substituting this into Eq. (14), together with $J=2\alpha(1-\alpha)$, the boundary between LL and SL is determined by

$$\left(\frac{1-\sqrt{1-4[2\alpha(1-\alpha)-\beta(1-\beta)]}}{2}\right)^2(1-\beta) = K\beta^2\left(1-\frac{1-\sqrt{1-4[2\alpha(1-\alpha)-\beta(1-\beta)]}}{2}\right). \quad (15)$$

2. Boundary between SL and HL

We study the value of $\frac{\partial \rho_B}{\partial x}|_{x=1}$ in regions HL and SL at sufficiently large Ω_A (we use $\Omega_A=1000$ here). It is found if we fix α and increase β, then $\frac{\partial \rho_B}{\partial x}|_{x=1}\to 0$ will be obtained on the boundary between HL and SL ($\beta=\beta_{c1}$) (see curve corresponding to $\beta=0.317$ in Fig. 8). When $\beta>\beta_{c1}$, $\frac{\partial \rho_B}{\partial x}|_{x=1}$ is positive. At another critical value $\beta=\beta_{c2}$, $\frac{\partial \rho_B}{\partial x}|_{x=1}$ becomes zero again. When $\beta>\beta_{c2}$, $\frac{\partial \rho_B}{\partial x}|_{x=1}$ is negative. In other words, there are two regions in the SL phase in which the sign of $\frac{\partial \rho_B}{\partial x}|_{x=1}$ is different. Suppose region A corresponds to positive sign and region B corresponds to negative sign. If we fix α and increase β, then HL first transits into region A and then transits into region B. HL does not transit into region B directly.

Based on this fact, the boundary between SL and HL could be obtained. Substituting $\frac{\partial \rho_B}{\partial x}|_{x=1}=0$ into Eq. (9) ("–" needs to be used because lane A is in low density), together with $J=2\alpha(1-\alpha)$ and $\rho_B|_{x=1}=1-\beta$, we have

$$\left(\frac{1-\sqrt{1-4[2\alpha(1-\alpha)-\beta(1-\beta)]}}{2}\right)^2\beta = K(1-\beta)^2\left(1-\frac{1-\sqrt{1-4[2\alpha(1-\alpha)-\beta(1-\beta)]}}{2}\right). \quad (16)$$

Figure 9 shows the curve corresponding to Eq. (16) (line E). It can be seen that the curve is paraboliclike. Numerical integration of the hydrodynamic equations shows that (i) HL either transits into region A or remains unchanged with the increase of β. (ii) If $\alpha>\alpha_{c1}$, region A always transits into region B with the increase of β. Here α_{c1} is horizontal coordinate of intersection point between line E and line $\beta=0.5$. (iii) Region B remains unchanged with the increase of β. Based on (i)–(iii), the boundary between SL and HL is de-

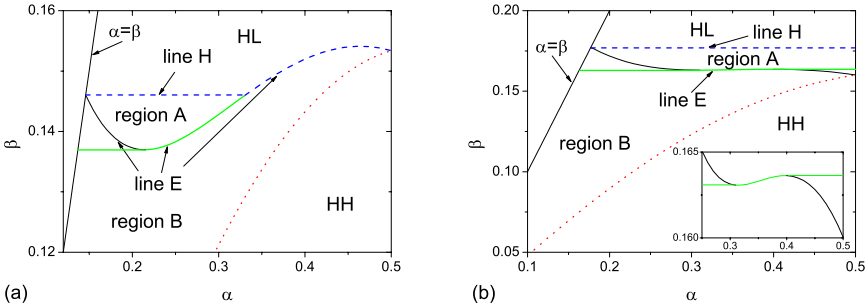

FIG. 10. (Color online) Boundary between HS and HL (blue dashed line). Boundary between HH and HS (red dotted line) is also shown, which is obtained from Eq. (18). (a) $K=0.005$; (b) $K=0.01$. The inset in (b) shows detail of line E and its tangent line.

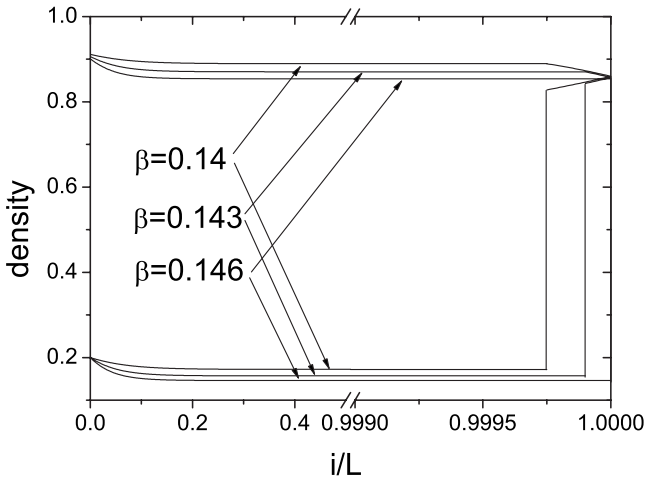

FIG. 11. Typical density profiles above curve E. The parameters are $\alpha=0.2, K=0.005, \Omega_A=1000$.

termined by curve E and its tangent line. Regions A and B are also determined by curve E and its tangent line, as shown in the figure. The arising of the tangent line means that the maximum flow rate that could be sustained in the SL phase is $J=2\alpha_{c2}(1-\alpha_{c2})$; here α_{c2} is the horizontal coordinate of the tangent line. Comparing Figs. 9(a) and 9(b), one can see that the boundary moves right and gradually becomes straight with increase of K.

3. Boundary between HH and HS

On the boundary between HH and HS, the density profile on lane A is flat at the left boundary, i.e., $\frac{\partial \rho_A}{\partial x}|_{x=0}=0$. Substituting this into Eq. (8) ("+" needs to be used because lane B is in high density), we have

$$\Omega_A \rho_A^2 \left(1-\frac{1+\sqrt{1-4[J-\rho_A(1-\rho_A)]}}{2}\right) = \Omega_B \left(\frac{1+\sqrt{1-4[J-\rho_A(1-\rho_A)]}}{2}\right)^2 (1-\rho_A). \quad (17)$$

Furthermore, we have $\rho_A|_{x=0}=1-\alpha$ and $J=2\beta(1-\beta)$ on the boundary. Substituting these into Eq. (17), the boundary between HH and HS is determined by

$$\left(1-\frac{1+\sqrt{1-4[2\beta(1-\beta)-\alpha(1-\alpha)]}}{2}\right)(1-\alpha)^2 = K\alpha\left(\frac{1+\sqrt{1-4[2\beta(1-\beta)-\alpha(1-\alpha)]}}{2}\right)^2. \quad (18)$$

4. Boundary between HS and HL

Similarly as in Sec. III C 2, we believe the boundary between HS and HL is relevant with $\frac{\partial \rho_A}{\partial x}|_{x=0}=0$. We substitute $\frac{\partial \rho_A}{\partial x}|_{x=0}=0$ into Eq. (8) (also "+" needs to be used because lane B is in high density); together with $\rho_A|_{x=0}=\alpha$ and $J=2\beta(1-\beta)$, we have

$$\left(1-\frac{1+\sqrt{1-4[2\beta(1-\beta)-\alpha(1-\alpha)]}}{2}\right)\alpha^2 = K(1-\alpha)\left(\frac{1+\sqrt{1-4[2\beta(1-\beta)-\alpha(1-\alpha)]}}{2}\right)^2. \quad (19)$$

Figure 10(a) shows the curve corresponding to Eq. (19) (line E) at $K=0.005$. The intersection point of the curve with line $\alpha=\beta$ can be solved. Substituting $\alpha=\beta$ into Eq. (19), we have

$$\left(1-\frac{1+\sqrt{1-4[2\beta(1-\beta)-\beta(1-\beta)]}}{2}\right)\beta^2 = K(1-\beta)\left(\frac{1+\sqrt{1-4[2\beta(1-\beta)-\beta(1-\beta)]}}{2}\right)^2, \quad (20)$$

which can be simplified into

$$\beta^3 = K(1-\beta)^3. \quad (21)$$

The solution is

$$\beta = \frac{K^{1/3}}{1+K^{1/3}}. \quad (22)$$

We note that above curve E, $\frac{\partial \rho_A}{\partial x}|_{x=0}$ is negative and below the curve, $\frac{\partial \rho_A}{\partial x}|_{x=0}$ is positive. We study the density profile above the curve. Figure 11 shows the density profiles with $\alpha=0.2$. It can be seen with the increase of β, the bulk density on lane B decreases. It is obvious that on the boundary between HS and HL ($\beta\approx 0.146$), $\frac{\partial \rho_B}{\partial x}|_{x=1}=0$ and $\rho_B|_{x=1}=1-\beta$. Substituting these into Eq. (9), together with $J=2\beta(1-\beta)$ ("−" needs to be used because lane A is in low density), we have

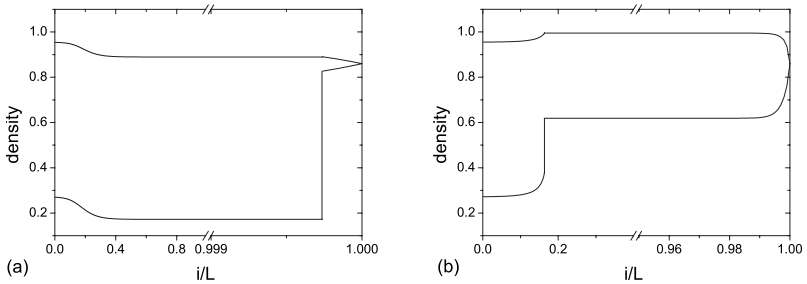

FIG. 12. Typical density profiles corresponding to $\beta=0.14$. Other parameters are $K=0.005$, $\Omega_A=1000$. (a) $\alpha=0.27$; (b) $\alpha=0.272$.

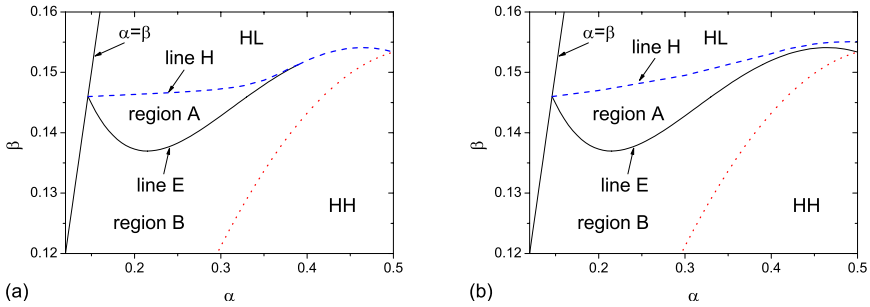

FIG. 13. (Color online) Boundary between HS and HL (blue dashed line). Boundary between HH and HS (red dotted line) is also shown, which is still obtained from Eq. (18) because Eq. (18) is valid provided $\Omega_A \gtrsim 15$. The parameters are $K=0.005$. (a) $\Omega_A=150$; (b) $\Omega_A=100$.

$$\left(\frac{1-\sqrt{1-4[2\beta(1-\beta)-\beta(1-\beta)]}}{2}\right)^2\beta = K(1-\beta)^2\left(1-\frac{1-\sqrt{1-4[2\beta(1-\beta)-\beta(1-\beta)]}}{2}\right), \tag{23}$$

which can be simplified into

$$\beta^3 = K(1-\beta)^3. \tag{24}$$

The equation is identical to Eq. (21). The solution is $\beta = \frac{K^{1/3}}{1+K^{1/3}}$.

The boundary between HS and HL is thus determined by curve E and line H corresponding to $\beta=\frac{K^{1/3}}{1+K^{1/3}}$ (blue line in Fig. 10). Numerical integration of the hydrodynamic equations shows that (i) if β is fixed and the increasing part of line E (symbolized by green color) is not crossed, changing α only affects density profile near the left end. (ii) In contrast, when across the increasing part of line E, the bulk densities on both lanes and the shock position will suddenly change (Fig. 12). Based on (i) and (ii), one knows that when across the tangent line of line E (also symbolized by green color), the bulk densities on both lanes and the shock position will also suddenly change. This is not observed in the model in Ref. [25].

With the increase of K, line H will gradually exceed the maximum value of curve E [see Fig. 10(b)]. In this case, the boundary between HS and HL is solely determined by line H: it becomes a straight line. With further increase of K, line E will become monotonically decreasing. As a result, the phenomenon as shown in Fig. 12 disappears.

Finally, we discuss curve E corresponding to Eq. (19) at small value of Ω_A. Figure 13(a) shows the phase boundaries with $\Omega_A=150$. In this case, Ω_A is not sufficiently large to obtain Eq. (24) and line H has to be determined numerically. Nevertheless, Eq. (19) is still valid. The boundary between HS and HL is still determined by line H and curve E. Figure 13(b) shows the phase boundaries with $\Omega_A=100$. In this case, line H does not intersect with curve E and the boundary between HS and HL is solely determined by line H. Although curve E is not relevant to the boundary any more, it is still valid: $\frac{\partial \rho_A}{\partial x}\big|_{x=0}$ is negative above curve E and it is positive below the curve. We also would like to point out that the phenomenon as shown in Fig. 12 also gradually disappears with the decrease of Ω_A. In Fig. 13, the bulk densities on both lanes and the shock position already change continuously when across the increasing part of line E and its tangent line.

5. Discontinuous lines

On the discontinuous line in the HS phase, density profile on lane A is flat in the bulk. Furthermore, $\rho_A=1/2$ in the bulk. Substituting these into Eq. (8) (note that "+" is used because lane B is in high density), together with $J=2\beta(1-\beta)$, the discontinuous line could be obtained,

$$\frac{1}{4}\left(1-\frac{1+\sqrt{1-4[2\beta(1-\beta)-0.25]}}{2}\right) = \frac{K}{2}\left(\frac{1+\sqrt{1-4[2\beta(1-\beta)-0.25]}}{2}\right)^2. \tag{25}$$

Similarly, on the discontinuous line in SL phase, the density profile on lane B is flat in the bulk. Furthermore, $\rho_B=1/2$ in the bulk. Substituting these into Eq. (9) (note that "−" is used because lane A is in low density), together with $J=2\alpha(1-\alpha)$, the discontinuous line could be obtained,

$$\frac{1}{2}\left(\frac{1-\sqrt{1-4[2\alpha(1-\alpha)-0.25]}}{2}\right)^2 = \frac{K}{4}\left(1-\frac{1-\sqrt{1-4[2\alpha(1-\alpha)-0.25]}}{2}\right). \tag{26}$$

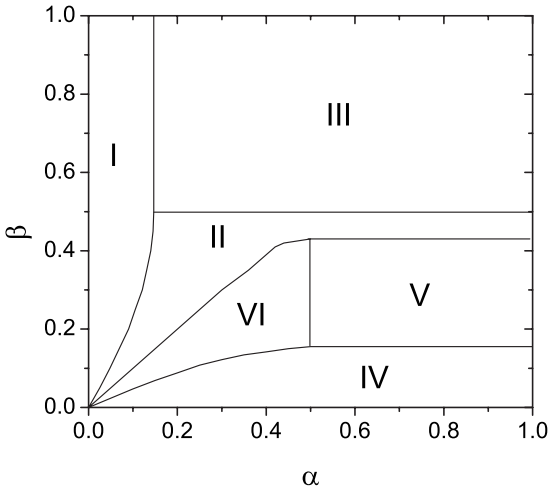

FIG. 14. Phase diagram corresponding to strong coupling. The parameters are $\omega_A=1$, $\omega_B=0$. System size is $L=10^4$.

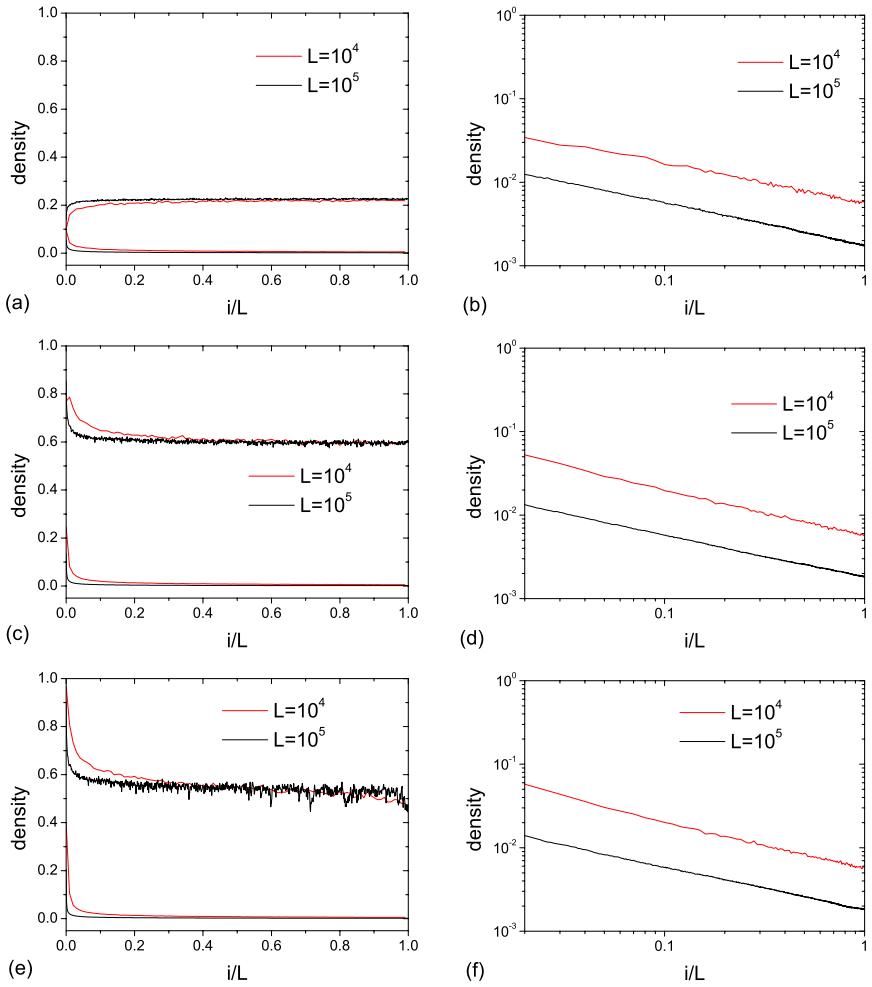

FIG. 15. (Color online) Density profiles in regions I–III. (a),(b) Region I, $\alpha=0.1$, $\beta=0.6$; (c),(d) Region II, $\alpha=0.25$, $\beta=0.4$; (e),(f) Region III, $\alpha=0.4$, $\beta=0.6$. In (b),(d),(f), density profiles on lane A is shown in the log-log plane.

The discontinuous line is a straight line in our model, while it is not in Ref. [25]. This is because in the HS and SL phase in our model, J is a function of α or β only. In contrast, in the HS and SL phase in Ref. [25], J is a function of α and β.

6. *Special cases $K=0$ and $K=1$*

The analytical results of phase boundaries and discontinuous lines are compared with those obtained by numerical integration. It is found that they are in good agreement (not shown). Now we consider two special cases, $K=0$ and $K=1$.

When $K=0$, Eqs. (15) and (16) become identical (note that we need to discard unreasonable solutions $\beta=0$ and $\beta=1$ for the two equations),

$$2\alpha(1-\alpha)=\beta(1-\beta), \tag{27}$$

which means SL disappears. Similarly, Eqs. (18) and (19) also become identical (note that we need to discard unreasonable solutions $\alpha=0$ and $\alpha=1$ for the two equations),

$$\alpha(1-\alpha)=2\beta(1-\beta), \tag{28}$$

which means HS disappears. Equations (27) and (28) are identical if interchanging α and β, which means symmetry of the phase diagram at $K=0$.

When $K=1$, it can be easily found out that the boundary (15) becomes $\alpha=\beta$. On the other hand, the boundary between SL and HL becomes $\alpha=0.5$ (This is fulfilled by studying the intersection point of Eq. (16) and line $\alpha=\beta$, which is $\alpha=\frac{K^{1/3}}{1+K^{1/3}}$.) This means SL disappears. Similarly, the boundary (18) becomes $\alpha=\beta$ and Eq. (22) becomes $\beta=0.5$. This

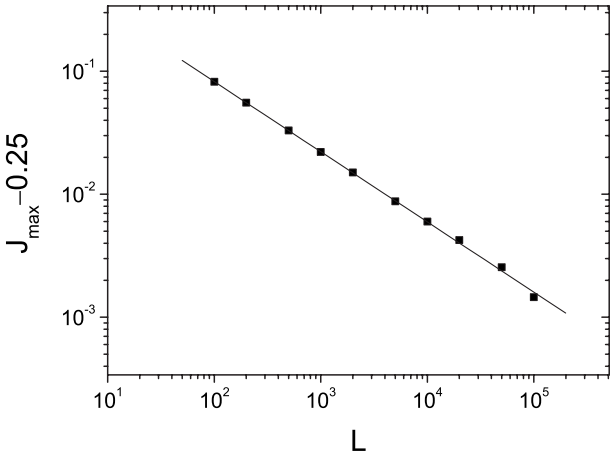

FIG. 16. The dependence of maximum flow rate J_{max} in region III on the system size. Note that $J_{max}-0.25$ is shown in the figure. The line is a guide for eyes.

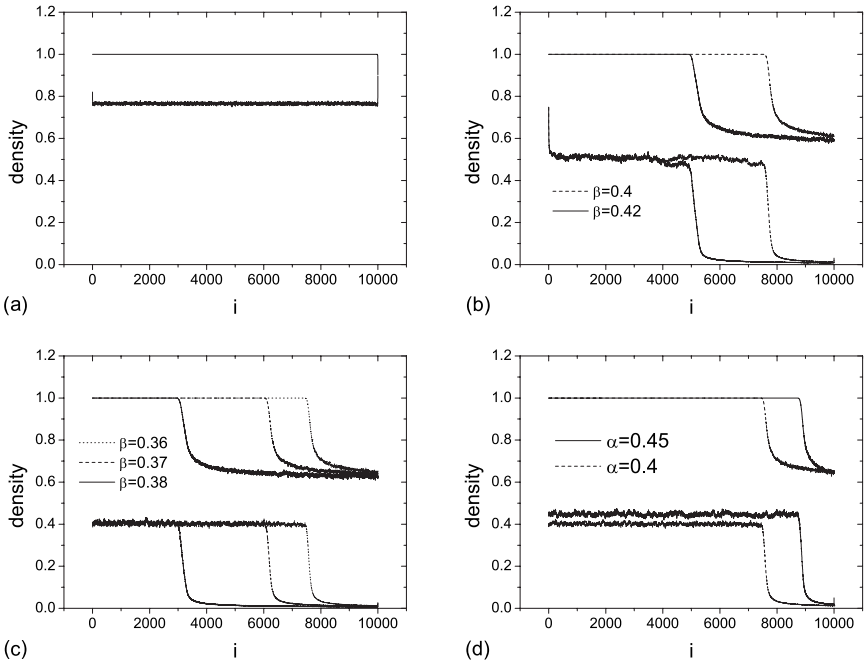

FIG. 17. Density profiles in regions IV–VI. (a) Region IV, $\alpha=1$, $\beta=0.1$; (b) region V, $\alpha=1$; (c),(d) region VI. In (c) $\alpha=0.4$; (d) $\beta=0.36$.

means HS disappears. As a result, our analytical results correctly reproduce the symmetry of the phase diagram at $K=1$.

IV. STRONG COUPLING

In this section, we study the situation arising from strong coupling, in which the lane changing rates ω_A and ω_B are independent of system size L.

A. $\omega_B=0$

In this subsection, we consider the case $\omega_B=0$. Before we carry out the Monte Carlo simulations, a cluster mean field analysis is presented as in Ref. [20]. Considering the sites far away from the boundaries, we assume that the occupation of vertical clusters is independent of the position along the lattice. We denote P_{11} as the probability to find a cluster with both sites filled, P_{10} (P_{01}) as the probability that the site on lane A (B) is filled and the site on lane B (A) is empty, and P_{00} as probability that both sites are empty.

The dynamics of the system could be described via the master equation. For P_{11}, we have

$$\frac{dP_{11}}{dt} = 2P_{10}P_{01} - 2P_{11}P_{00}. \tag{29}$$

For P_{10}, we have

$$\frac{dP_{10}}{dt} = -2P_{10}P_{01} + 2P_{11}P_{00} + \omega_B P_{01}(P_{01} + P_{11}) - \omega_A P_{10}(P_{10} + P_{11}). \tag{30}$$

In the steady state, $\frac{dP_{11}}{dt} = \frac{dP_{10}}{dt} = 0$, together with $\omega_B=0$, we have

$$P_{10}P_{01} = P_{11}P_{00}, \tag{31}$$

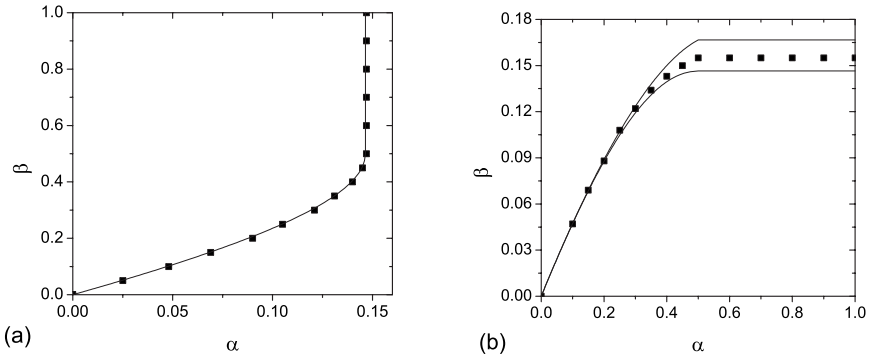

FIG. 18. (a) Phase boundary between region I and regions II and III; (b) phase boundary between region IV and regions V and VI. The scattered data are simulation results in the system with $L=10^4$. The line in (a) is the analytical approximation Eq. (35), the bottom line in (b) is the analytical approximation Eq. (36), the other line in (b) is the mean field approximation result presented in Ref. [20].

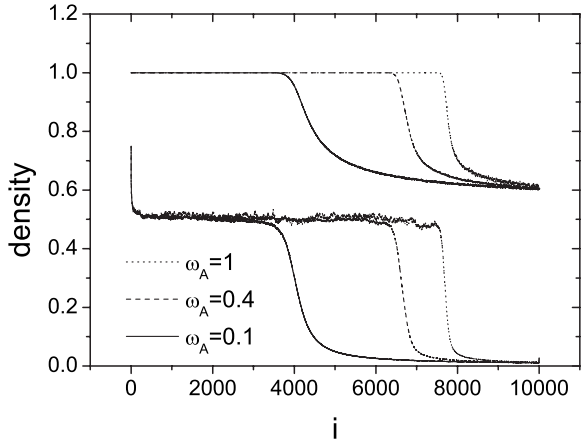

FIG. 19. Density profiles at different values of ω_A. The parameters are $\alpha=1$, $\beta=0.4$.

$$P_{10}(P_{10}+P_{11})=0. \tag{32}$$

This leads to

$$P_{10}=P_{11}=0 \tag{33}$$

or

$$P_{10}=P_{00}=0. \tag{34}$$

Equations (33) and (34) are exactly the same as Eqs. (11) and (12) in Ref. [20]. Therefore a naive expectation is that the same results could be obtained, i.e., the phase diagram should be classified into seven phases as in the model of Pronina and Kolomeisky (see Fig. 3 in Ref. [20]) and the corresponding density profiles are also similar to that in Ref. [20]. Nevertheless, it is not the case as shown below, and we argue that this is because the boundary plays an important role in our system.

Figure 14 shows the phase diagram with system size $L=10^4$ and $\omega_A=1$. The phase diagram is classified into six regions. Figure 15(a) shows a typical density profile in region I. It can be seen that lane B is in low density ($\rho_B<0.5$). Figure 15(b) shows density profile on lane A in a log-log plane. It can be seen the density profile decays in power law. Furthermore, the slope at a different system size is the same. This is different from the results in Ref. [20], where zero density on lane A could be observed even in a small sized system.

Figures 15(c) and 15(d) show a typical density profile in region II, in which lane B is in high density ($\rho_B>0.5$). The density profile on lane A also decays in power law. This phase is therefore named the decay-high density (D-HD) phase.

Figures 15(e) and 15(f) show a typical density profile in region III. The density profile on lane A still decays in power law. Our simulations show that the maximum flow rate of the system is reached in this region and the maximum flow rate decreases with the increase of system size. Figure 16 shows it decays toward 0.25 in power law.

In region IV, high density is observed on lane A and the density on lane B equals 1 [Fig. 17(a)]. This phase is also observed in Ref. [20] and is named HD-1.

Region V corresponds to a coexistence phenomenon [Fig. 17(b)]. In the left bulk, the system is in MC-1 phase, i.e., the maximum current 0.25 is observed on lane A and the density on lane B equals 1. In the right bulk, D-HD phase is observed. The width of the D-HD phase depends on β. With the increase of β, the D-HD phase expands [Fig. 17(b)]. When $\beta\to0.5$, the D-HD phase tends to be infinitely wide. This means in an infinite system, regions V and III are separated by $\beta=0.5$ instead of by region II. In a finite system, when the width of D-HD phase approaches system size, the MC-1 phase will be driven out of the system and the coexistence phenomenon will transit into the pure D-HD phase.

Region VI also corresponds to a coexistence phenomenon [Figs. 17(c) and 17(d)]. In the left bulk, the system is in the LD-1 phase, i.e., low density is observed on lane A and the density on lane B equals 1. In the right bulk, the D-HD phase is observed. The width of the D-HD phase increases with the increase of β [Fig. 17(c)] and it also increases with the decrease of α [Fig. 17(d)]. Therefore the coexistence phenomenon transits into the pure D-HD phase with the increase of β and/or with the decrease of α.

We study the phase boundary between region I and regions II and III. It can be seen from Fig. 15(a) that $\rho_A|_{x=0}\approx\rho_B|_{x=0}\approx\alpha$ and $J_A|_{x=1}\approx0$ in region I. As a result, the boundary could be approximated by

$$2\alpha(1-\alpha)=\min(\beta(1-\beta),0.25). \tag{35}$$

Figure 18(a) shows that the analytical approximation is in good agreement with simulation results. However, the phase boundary between region IV and regions V and VI could not be determined in a similar way because although we have $J_B|_{x=0}=0$, we do not have $\rho_A|_{x=1}\approx\rho_B|_{x=1}\approx1-\beta$ in region

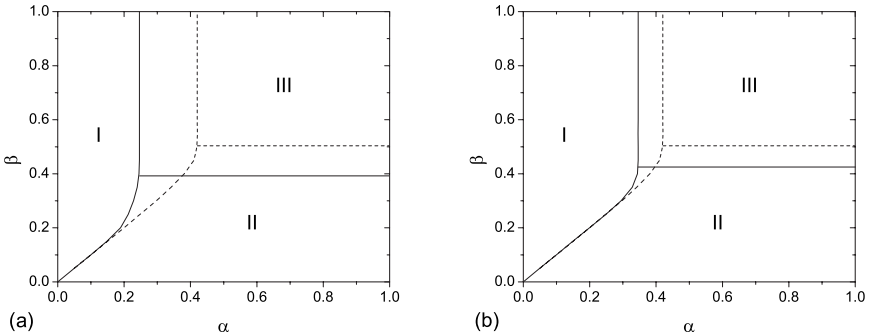

FIG. 20. (a) Phase diagram at $\omega_A=1$, $\omega_B=0.01$ (solid lines), $\omega_B=0.1$ (dashed lines); (b) phase diagram at $\omega_A=0.1$, $\omega_B=0.01$ (solid lines), $\omega_A=1$, $\omega_B=0.1$ (dashed lines). System size is $L=1000$.

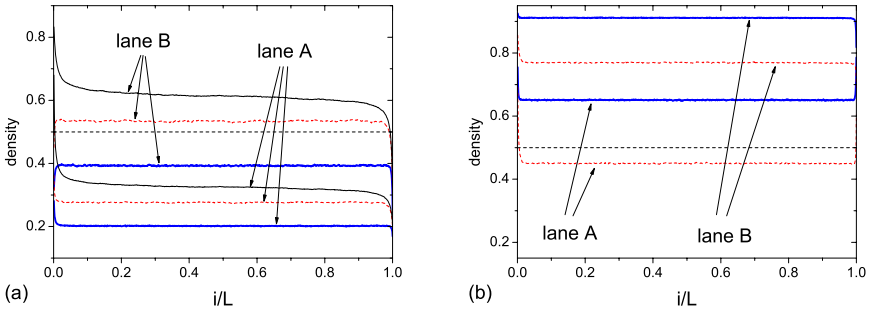

FIG. 21. (Color online) Typical density profiles at $\omega_B=0.1$. System size $L=1000$, the parameter is $\omega_A=1$. (a) Black curves correspond to region III and the parameters are $\alpha=1$, $\beta=1$, red and blue curves correspond to region I, and the parameters are $\alpha=0.4$ (red dashed), $\alpha=0.3$ (blue thick), $\beta=1$; (b) curves correspond to region II and the parameters are $\alpha=1$, $\beta=0.35$ (red dashed), $\beta=0.2$ (blue thick).

IV. Figure 18(b) shows that the simulation results deviate from analytical approximation,

$$2\beta(1-\beta)=\min(\alpha(1-\alpha),0.25). \tag{36}$$

Moreover, the mean field approximation result presented in Ref. [20] also deviates from the simulation results.

With the increase of system size, the boundary between regions V and II moves upward, the boundary between regions VI and II moves accordingly and gradually becomes straighter, other boundaries do not change. We would like to mention that the boundary between regions V and II never reaches $\beta=0.5$ in a finite system, because the D-HD phase tends to be infinitely wide when $\beta\to 0.5$.

With the decrease of ω_A, the boundary between regions V and II moves downward because the width of the D-HD phase increases (Fig. 19). The boundary between regions VI and II moves accordingly. The boundary between region IV and regions V and VI also moves downward and gradually approaches the curve determined by Eq. (36), because $\rho_A|_{x=1}$ and $\rho_B|_{x=1}$ gradually approach $1-\beta$. Other boundaries do not change.

B. $\omega_B>0$

In this subsection, we study the case $\omega_B>0$. It is found that the power law decay behavior on lane A disappears. The density profiles on both lanes are flat in the bulk. Moreover, the coexistence phenomenon also disappears. Figure 20(a) shows the phase diagram at $\omega_A=1$, which is classified into three regions. In region I (II), the system is in the entry (exit) dominated phase. The flow rate increases with the increase of α (β) and is independent of β (α). In region III, maximum flow rate is reached in the system. The phase transition from region I to region II is of first order, with jumps of bulk densities on both lanes. The phase transition from region III to region I or region II is continuous.

We study the bulk densities on lanes A and B. The typical density profiles are shown in Fig. 21. In region III, lane A is in low density and lane B is in high density [see black curves in Fig. 21(a)]. In region I, lane A is in low density and ρ_A increases with the increase of α. ρ_B also increases with the increase of α. Nevertheless, it will exceed 0.5 when α is large [see red curves in Fig. 21(a)]. In region II, lane B is in high density and ρ_B decreases with the increase of β. ρ_A also decreases with the increase of β. Nevertheless, it will be smaller than 0.5 when β is large [see red curves in Fig. 21(b)].

With the increase of ω_B, regions I and II expand and region III shrinks [Fig. 20(a)]. Figure 22 shows that the maximum flow rate in region III increases with the increase of ω_B. When ω_B is large, the maximum flow rate will exceed 0.5, which is two times the maximum flow rate of single lane ASEP. This means the lane changing behavior in our model could either enhance or reduce flow rate, depending on the lane changing rates.

This result is different from that of the model proposed in Ref. [20]. We have performed simulations of the model in Ref. [20], it is found that the maximum flow rate never exceeds 0.5. This difference is due to that the correlation effect between neighbor vertical clusters could not be neglected in our model. In contrast, the correlation effect is trivial and could be neglected in the model in Ref. [20].

We also study the effect of ω_A. Figure 20(b) shows that when ω_B/ω_A is fixed, regions I and II expand and region III shrinks with the increase of ω_A. Figure 21 shows that the maximum flow rate decreases with the decrease of ω_A in our model.

V. CONCLUSION

In this paper, we have studied a two-lane totally asymmetric simple exclusion process, in which particles could jump

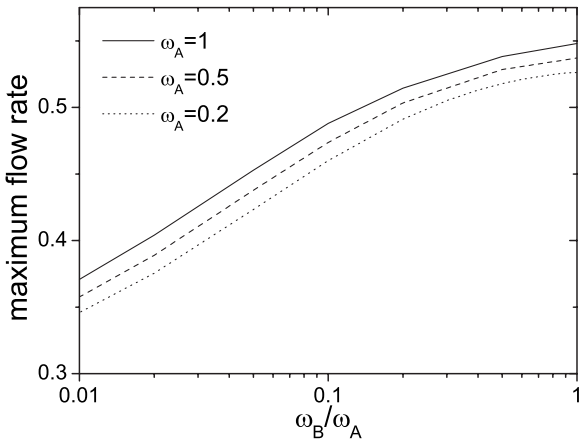

FIG. 22. Maximum flow rate in our model. System size is $L=1000$.

between the two lanes with asymmetric rates. We have investigated both the weak coupling situation and the strong coupling situation.

In the weak coupling situation, the density profiles and phase diagrams are constructed in the hydrodynamic limit, by numerically solving the steady state equations. The results are in good agreement with Monte Carlo simulations. The appearance of localized shock in one lane and the discontinuous phase transition as revealed by Juhász [25] are also reproduced. However, the phase diagram in our model exhibits asymmetry, which is different from the symmetric one in Juhász's model. We have studied the phase boundary and discontinuous line analytically. The analytical results are in good agreement with that obtained from numerical integration.

In the strong coupling situation, the shock does not exist anymore. We also found that the results are qualitatively different between $\omega_B=0$ and $\omega_B>0$. When $\omega_B=0$, the phase diagram consists of six regions, which is different from that of the model presented by Pronina and Kolomeisky [20]. It is also shown that in the case of $\omega_B>0$, flow rates larger than 0.5 could be observed in our model due to correlation effect between neighbor vertical clusters.

ACKNOWLEDGMENTS

This work was supported by the National Basic Research Program of China (Grant No. 2006CB705500), the NNSFC under Project Nos. 10532060, 10404025, 70601026, and 10672160, the CAS President Foundation, the Chinese Postdoc Research Foundation (Grant No. 20060390179), the NCET, and the FANEDD. Y.-H. Wu acknowledges the support of the Australian Research Council through a Discovery Project Grant.

[1] B. Derrida, Phys. Rep. **301**, 65 (1998); R. A. Blythe and M. R. Evans, J. Phys. A **40**, R333 (2007).
[2] G. M. Schütz, in *Phase Transitions and Critical Phenomena*, edited by C. Domb and J. L. Lebowitz (Academic Press, San Diego, 2001), Vol. 19, pp. 1–251.
[3] J. T. MacDonald, J. H. Gibbs, and A. C. Pipkin, Biopolymers **6**, 1 (1968).
[4] G. M. Schütz, Europhys. Lett. **48**, 623 (1999).
[5] T. Chou, Phys. Rev. Lett. **80**, 85 (1998).
[6] B. Widom, J. L. Viovy and A. D. Defontaines, J. Phys. I **1**, 1759 (1991).
[7] S. Klumpp and R. Lipowsky, J. Stat. Phys. **113**, 233 (2003); R. Lipowsky, S. Klumpp, and T. M. Nieuwenhuizen, Phys. Rev. Lett. **87**, 108101 (2001).
[8] L. B. Shaw, R. K. P. Zia, and K. H. Lee, Phys. Rev. E **68**, 021910 (2003).
[9] D. Chowdhury, L. Santen, and A. Schadschneider, Phys. Rep. **329**, 199 (2000).
[10] D. Helbing, Rev. Mod. Phys. **73**, 1067 (2001).
[11] K. Nishinari, Y. Okada, A. Schadschneider, and D. Chowdhury, Phys. Rev. Lett. **95**, 118101 (2005); P. Greulich, A. Garai, K. Nishinari, A. Schadschneider, and D. Chowdhury, Phys. Rev. E **75**, 041905 (2007).
[12] A. Parmeggiani, T. Franosch, and E. Frey, Phys. Rev. Lett. **90**, 086601 (2003).
[13] A. Parmeggiani, T. Franosch, and E. Frey, Phys. Rev. E **70**, 046101 (2004).
[14] M. R. Evans, R. Juhász, and L. Santen, Phys. Rev. E **68**, 026117 (2003).
[15] V. Popkov, A. Rakos, R. D. Willmann, A. B. Kolomeisky, and G. M. Schutz, Phys. Rev. E **67**, 066117 (2003).
[16] V. Popkov and I. Peschel, Phys. Rev. E **64**, 026126 (2001); V. Popkov and G. M. Schütz, J. Stat. Phys. **112**, 523 (2003).
[17] E. Pronina and A. B. Kolomeisky, J. Phys. A **37**, 9907 (2004).
[18] R. J. Harris and R. B. Stinchcombe, Physica A **354**, 582 (2005).
[19] T. Mitsudo and H. Hayakawa, J. Phys. A **38**, 3087 (2005).
[20] E. Pronina and A. B. Kolomeisky, Physica A **372**, 12 (2006).
[21] R. Jiang, R. Wang, and Q. S. Wu, Physica A **375**, 247 (2007).
[22] T. Reichenbach, T. Franosch, and E. Frey, Phys. Rev. Lett. **97**, 050603 (2006); T. Reichenbach, E. Frey, and T. Franosch, New J. Phys. **9**, 159 (2007).
[23] H.-W. Lee, V. Popkov, and D. Kim, J. Phys. A **30**, 8497 (1997).
[24] M. E. Fouladvand and H. W. Lee, Phys. Rev. E **60**, 6465 (1999).
[25] R. Juhász, Phys. Rev. E **76**, 021117 (2007).
[26] Note that localized shock is also found in Ref. [22] in a unidirectional model. However, the lane changing is symmetric in the model. The shock is induced due to unequal injection rates and removal rates.
[27] We would like to mention that in the model in Ref. [25], the total current J needs to be obtained iteratively in the HH phase and the LL phase. Moreover, $J=\alpha(1-\alpha)-\beta(1-\beta)$ in HL, HS, and SL phases in Ref. [25]. In Ref. [25], analysis of the phase boundary between HH and HS as well as the phase boundary between SL and LL is more complicated. Similarly, as shown in the following text, analysis of the phase boundary between HL and HS as well as the phase boundary between SL and HL is more complicated in our model.